Xu, Q., Zhao, J., Yuan, X., Liu, H., Ju, C., Schurr, B., Bloch, W. (2021): Deep Crustal Contact Between the Pamir and Tarim Basin Deduced From Receiver Functions. - Geophysical Research Letters, 48, 9, e2021GL093271.

https://doi.org/10.1029/2021GL093271

Geophysical Research Letters

RESEARCH LETTER
10.1029/2021GL093271

Key Points:

- The Asian lower crust is delaminated beneath the central east Pamir
- The northeast Pamir crust extends into the Tarim Basin and thickens by pure shear shortening
- The southeast Pamir crust is underthrusting beneath West Kunlun Shan and Tarim Basin

Supporting Information:

Supporting Information may be found in the online version of this article.

Correspondence to:

Q. Xu and J. Zhao,
xuqiang@itpcas.ac.cn;
zhaojm@itpcas.ac.cn

Citation:

Xu, Q., Zhao, J., Yuan, X., Liu, H., Ju, C., Schurr, B., & Bloch, W. (2021). Deep crustal contact between the Pamir and Tarim Basin deduced from receiver functions. *Geophysical Research Letters*, *48*, e2021GL093271. https://doi.org/10.1029/2021GL093271

Received 6 MAR 2021
Accepted 21 APR 2021

Deep Crustal Contact Between the Pamir and Tarim Basin Deduced From Receiver Functions

Qiang Xu[1], Junmeng Zhao[1], Xiaohui Yuan[2], Hongbing Liu[1], Changhui Ju[1], Bernd Schurr[2], and Wasja Bloch[2]

[1]State Key Laboratory of Tibetan Plateau Earth System Science (LATPES), Institute of Tibetan Plateau Research, Chinese Academy of Sciences, Beijing, China, [2]Deutsches GeoForschungsZentrum GFZ, Telegrafenberg, Potsdam, Germany

Abstract The deep crustal deformation in the east Pamir in response to the Cenozoic collision with the Tien Shan and the Tarim Basin is so far poorly constrained. We present new insights into the crustal structure of the east Pamir and its surrounding regions using P receiver functions from 40 temporary and permanent seismic stations. The crustal thickness reaches a maximum of 88 km beneath the central and southern east Pamir and decreases sharply to 50–60 km along the southern Tien Shan and to 41–50 km below the Tarim Basin. The most prominent crustal structures involve a double Moho, suggesting eastward underthrusting of the Pamir lower crust beneath southern east Pamir, and two Moho offsets, supporting delamination of Asian lower crust below the central east Pamir and pure shear shortening along the northeastern margin between the Pamir and Tarim Basin.

Plain Language Summary The Pamir orogen is located at the leading edge of the Indo-Asian collision zone and has translated northward by about 300 km with respect to the Himalaya-Tibetan plateau since the Late Cenozoic. It protruded the formerly connected Tajik and Tarim basins and formed a curviplanar front with the Tajik Basin to the west, Tien Shan to the north, and Tarim Basin to the east. Previous studies revealed that the Pamir is underthrusted by the Asian crust from the west and the north; however, it is still unclear how the contact between Pamir and the Tarim basin crust looks like. This study elucidates the deep crustal interaction between the two tectonic blocks by receiver functions with data from a recent seismic experiment in the region. The Pamir crust is extended into the western tip of the Tarim basin and is thickened by horizontal shortening, while in the south it is underthrusting beneath the West Kunlun Shan and Tarim Basin into the mantle to a depth of >100 km.

1. Introduction

The Pamir orogen lies north of the western Himalayan syntaxis in the India-Asia collision zone (Figure 1) and attains an elevation of ≥4 km and a maximum crustal thickness of nearly 90 km by absorbing ~55–64% Cenozoic shortening within a relatively narrow north-south distance compared to the Tibetan Plateau (Schmidt et al., 2011; Schneider et al., 2019). A major orocline has formed due to the northward displacement of the Pamir by at least 300 km relative to the Tibet and Hindu Kush, with bending of this orogen associated with several well-developed thrusting and strike-slip faults along its margins (Figure 1) (Burtman & Molnar, 1993); these include the sinistral Darvaz strike-slip fault bounding the Tajik Basin to the west, the dextral Kashgar-Yecheng Transfer System (KYTS) bounding the Tarim Basin to the east and the Main Pamir Thrust System (MPT) bounding the Alai Valley to the north (Figure 1). The Pamir can be divided into the North, Central, and South Pamir, which are separated by the Tanymas and Rushan-Pshart sutures (Schwab et al., 2004). Structurally, the Central and South Pamir comprises terranes of Gondawana origin, whereas the North Pamir and West Kunlun Shan (WKS) are of Asian affinity (Li et al., 2020).

Intense intermediate-depth seismicity has been observed beneath the Pamir and Hindu Kush (Pegler & Das, 1998; Sippl et al., 2013), which is interpreted as evidence for ongoing intracontinental subduction (Schneider et al., 2013; E. R. Sobel et al., 2013) or forced delamination (Kufner et al., 2016). The opposite dips of deep earthquakes beneath the Pamir and Hindu Kush have invoked different interpretations about the plate configuration ranging from a single contorted slab of Indian (Pegler & Das, 1998), or Asian origin (Perry et al., 2019) to a two-slab model that involves the eastward to southward subduction/delamination

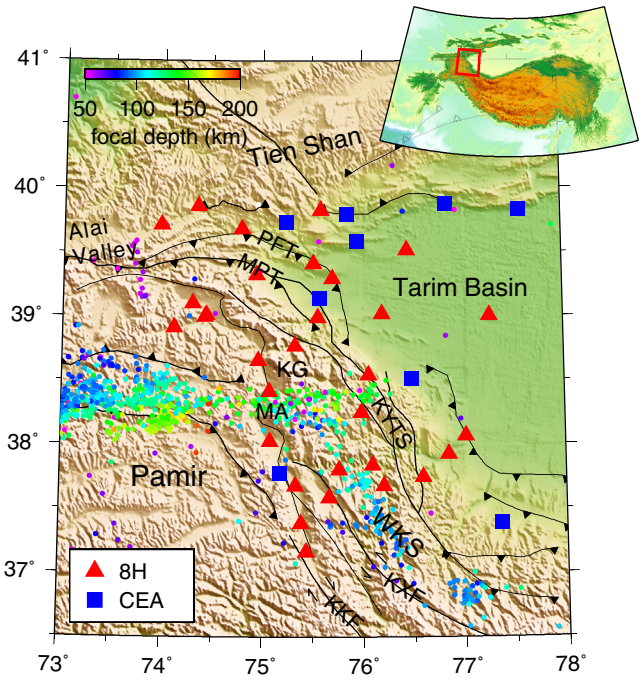

Figure 1. Topographic map of East Pamir showing simplified faults and locations of the seismic stations. The red triangles represent 8H stations, and the blue squares denote the CEA permanent stations. The color-coded dots mark the intermediate-depth earthquakes at depths greater than 50 km (Bloch et al., 2021). The top right inset illustrates the location of our study region (red box) relative to the India-Asia collision zone. KG, Kongur Shan; KKF, Karakoram fault; KXF, Karakax fault; KYTS, Kashgar-Yecheng Transfer System; MA, Muztagh Ata; MPT, Main Pamir Thrust; PFT, Pamir Frontal Thrust; WKS, West Kunlun Shan.

of Asian lithosphere in a tight 90° arc beneath the Pamir and northward subduction of Indian lithosphere beneath the Hindu Kush (Burtman & Molnar, 1993; Kufner et al., 2016; Negredo et al., 2007). A receiver function image along a north-south profile at ~73.8° E reveals that these intermediate-depth earthquakes occur in a 10–15 km thick low velocity zone possibly associated with the southward subduction of Asian lower crust reaching a depth of 150 km (Schneider et al., 2013), consistent with the results of local earthquake tomography and guided waves analyses (Mechie et al., 2019; Sippl et al., 2013). Recently, an additional NW-SE trending intermediate-depth earthquake zone has been identified south of the eastern termination of the E-W striking segment of the Pamir seismic zone (Bloch et al., 2021), roughly parallel to the WKS, which suggests a different tectonic origin compared to the Pamir-Hindu Kush seismic zone.

A previous receiver function analysis shows a double Moho structure at 50–90 km depth in both the western and central Pamir, which hints at underthrusting of the Tajik and Alai lower crust beneath western Pamir (Schneider et al., 2013, 2019). Plate motion vectors, shear-wave velocity and radial anisotropy models, and seismotectonic analysis testify that crustal materials flow outward from the interior of the Pamir toward the western flanks and/or extrude upward along with a series of thrust faults (Liang et al., 2020; Metzger et al., 2020; Schurr et al., 2014). Conversely, the more rigid Tarim crust may hinder the eastward extrusion of the east Pamir (Metzger et al., 2020; Schurr et al., 2014). The dextral KYTS as the boundary between the east Pamir and Tarim Basin is supposed to be the eastern edge of subducting Asian lithosphere (E. R. Sobel et al., 2013). However, how the crust deforms in the east Pamir facing the obstruction of the Tarim Basin remains insufficiently constrained, partly due to limited data available in this region.

In this study, we employ P receiver functions (PRFs) derived from a recently deployed temporary seismic array and permanent stations to investigate the crustal structure beneath the eastern Pamir and its adjacent region at a higher resolution than has previously been possible. Our observations of the crustal thickness and Vp/Vs ratio provide new insights into the crustal deformation patterns in the east Pamir under the resistance of Tarim Basin and Tien Shan during intracontinental orogenesis.

2. Data and Methods

The three-component seismograms used in this study were recorded at 40 broadband stations during the period from 2015 to 2017, consisting of 31 stations in a temporary two-dimensional (2-D) seismic array of the east Pamir seismic experiment (FDSN code 8H (Yuan et al., 2018); and nine permanent stations from China Earthquake Administration network (Zheng et al., 2010) (Figure 1). We selected teleseismic earthquakes with signal-to-noise ratios on the vertical component ≥2.5, body-wave magnitudes (Mb) ≥5.5, and epicentral distances of 30–95° for the PRF computations.

PRF analysis is one of the most frequently used techniques to explore seismic structures underneath a seismic station using the P-to-S (Ps) conversions and associated multiples that originate from discontinuities at different depths. The raw Z-N-E traces of each event are rotated into the ray-based P-SV-SH coordinate system using the theoretical back azimuth and incident angle. The P component is then deconvolved from the SV component using a time-domain Wiener filtering method to produce the SV receiver function (PRF) (Yuan et al., 1997). Visual quality control was carried out on all of the PRFs to eliminate outliers with significant oscillations or strong amplitudes. Finally, a total of 3,153 PRFs, obtained from 270 teleseismic events, were retained for subsequent processing.

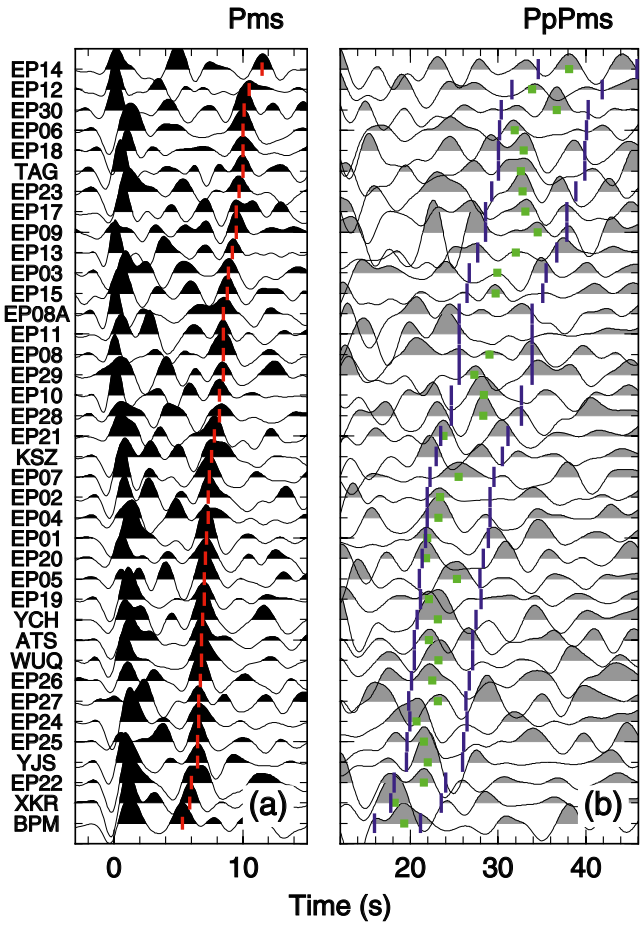

Figure 2. Stacks of PRFs for each station with moveout corrections already completed for (a) Ps and (b) PpPs sorted by the delay time of the Moho Ps conversion. The red ticks and green squares delineate the picked arrivals of the Moho Ps and PpPs phases, respectively. The blue ticks mark the predicted time windows for the appearance of the PpPms phase at each station. PRF, P receiver functions.

We estimate the crustal thickness (H) and Vp/Vs ratio (κ) at each station using the delay times of the Moho Ps and PpPs phases (Xu et al., 2017). This algorithm avoids the effects of multiple extremes on the energy surface that are often confronted by the popular H-κ stacking method in complex orogenic areas (Murodov et al., 2018; Zhu & Kanamori, 2000), thereby yielding more robust solutions for H and κ. We manually pick both delay times on two individual sum traces that are produced by stacking all of the PRFs from each station after a moveout correction for the Ps and PpPs phases, respectively. To identify the PpPs phase reliably, we pick this phase within a predicted time window based on the picked delay time of the Moho Ps conversion and two κ values of 1.6 and 2.0. The two standard deviations obtained using the bootstrap resampling technique (Xu et al., 2017), are considered as the uncertainties for both H and κ (Table S1).

To delineate the morphology of the subsurface discontinuities, three cross-sections are constructed using a common conversion point (CCP) stacking technique (e.g., Yuan et al., 2000) (See supporting informaiton Text S1). In addition, we also obtain the 1-D crustal Vs models by forwarding modeling the PRFs stacks for six key stations located in the Moho depth anomalous regions along with three profiles. Synthetic PRFs are calculated from 1-D velocity models using the reflectivity method with a ray parameter of 6.4 s/° (Yuan et al., 1997).

3. Results

Figure 2 exhibits PRF stacks for 38 stations, together with the carefully picked delay times of the Moho Ps and PpPs phases. The Moho Ps and PpPs conversions arrive at 5.3–11.5 s and 18.2–38.1 s, respectively. Stations KSH and EP16 (Figure S1) are not included due to ambiguous Moho Ps signals caused by strong sedimentary reverberations. We simultaneously obtain H and κ values for 35 stations, for which both the Moho Ps and PpPs are clearly visible. For three other stations, we could not determine the κ values because the Moho PpPs phases are unclear. We only estimate the H values using the arrival times of the Moho Ps conversions and κ values from their adjacent stations (Table S1).

We generate a regional-scale crustal thickness map across the Pamir and its surrounding region by combining previously published results with the measurements obtained in this study (Table S2 and Figure 3a). Details of crustal thickness variations outside our study region can be found in Schneider et al. (2019) and Zhang et al. (2020). The map reveals two deep Moho regions (called here Moho troughs), one in the western and central Pamir along the boundary region of the Pamir with the Tajik Basin and Alai Valley (Schneider et al., 2019), the other in the east Pamir along the WKS, the boundary region with the Tarim Basin. Both Moho troughs are parallel to intermediate-depth seismic zones. In this paper, we focus on our observations in the eastern Pamir. The resulting H values decrease from 67-88 km beneath the east Pamir to 50–60 km along the southern Tien Shan and 41–50 km beneath the Tarim Basin. The thickest crust (up to 88 km) is observed in the southeastern Pamir along the West Kunlun Shan and an elongated region of thicker crust with a thickness ranging from 68 to 74 km in the northeastern margin of the Pamir extends northeastward to the Pamir Frontal Thrust (PFT). Figure 3b indicates that the κ values vary significantly, ranging from 1.68 to 1.89 with an average uncertainty of 0.02.

Strong positive conversions at depths of 40–90 km, which are interpreted to be indicative of the Moho, are clearly identified in the CCP stacking images along three selected cross-sections (Figure 4). Superimposing the crustal thicknesses over the three CCP images reveals a good agreement with the lateral variations in

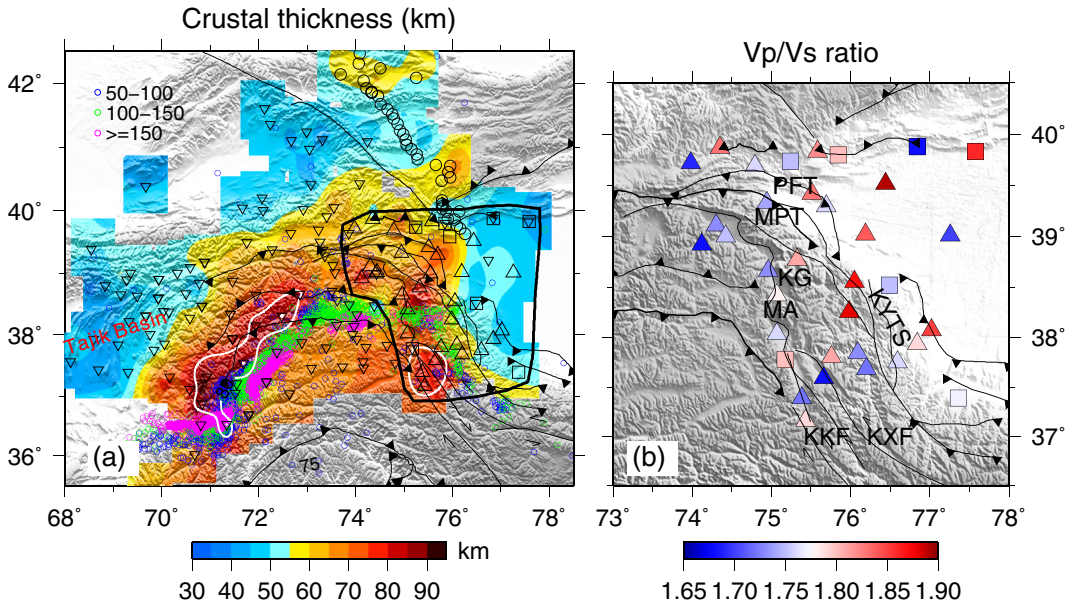

Figure 3. Maps of the (a) crustal thickness and (b) average Vp/Vs ratio. The crustal thickness values from Schneider et al. (2019) and Zhang et al. (2020) have also been included in Figure 3a. The intermediate-depth earthquakes at depths greater than 50 km from Bloch et al. (2021) are marked in Figure 3a by color-coded circles. The results for the area delineated by the black line in Figure 3a are analyzed in detail in this study. The white lines in Figure 3a outline the two Moho troughs.

Moho depth, giving confidence that the imaged Moho structure is robust. A Moho offset of at least 12 km appears below the surface trace of the PFT along profile A-A′, separating a sub-horizontal Moho at depths of 70–78 km in the south from a shallowly south-dipping Moho at 50–58 km depth in the north. Profile C-C′ is characterized by another significant Moho offset of about 18 km below Muztagh Ata (MA); this offset separates a south-dipping Moho at 60–88 km depth in the north from a sub-horizontal Moho at 70–78 km depth in the south. A double Moho structure is observed below the surface trace of the KXF along profile B-B′; the deeper Moho reaches a depth of 88 km and continues to dip eastward, while the shallower Moho at depths of 62–66 km gradually shallows to 45 km beneath the Tarim Basin. The individual PRFs at stations EP29 and EP30 (Figure S1) which are located above this double structure are shown in Figure S2. These key observations are supported by the Vs models obtained from the waveform modeling (Figures S3–S5).

4. Discussion

The most striking features observed in our CCP stacking images are the presence of a double Moho structure and two Moho offsets, which contribute fresh insights into the dynamic processes of crustal deformation in the eastern Pamir and its surrounding region. Figure 5 summarizes our structural interpretation of the imaged crustal structure.

The Moho offset observed below the PFT in the northeastern (NE) Pamir marks the tectonic boundary between the Pamir and the Tarim Basin. In the tectonic context of northward indentation of the Pamir and resistance of the strong Tarim lithosphere, the development of the Moho offset suggests that pure shear shortening is responsible for the crustal thickening in the NE Pamir. On both sides of this Moho offset, the Vs models of station EP23 in the NE Pamir to the south and station KSZ in the Tarim Basin to the north (Figure S3), as well as the Vp model from a wide-angle seismic transect (X. K. Zhang et al., 2002), clearly show that the middle-lower crust of the NE Pamir is significantly thicker than that of the Tarim basin. This observation correlates well with the feature of pure shear shortening, which can be considered as the direct evidence to support our interpretation. This interpretation is also consistent with stratigraphic and magnetostratigraphic data, suggesting the topographic uplift and exhumation of the NE Pamir since the Pliocene which cause the deformation front of the NE Pamir margin to migrate northward from the MPT to the PFT

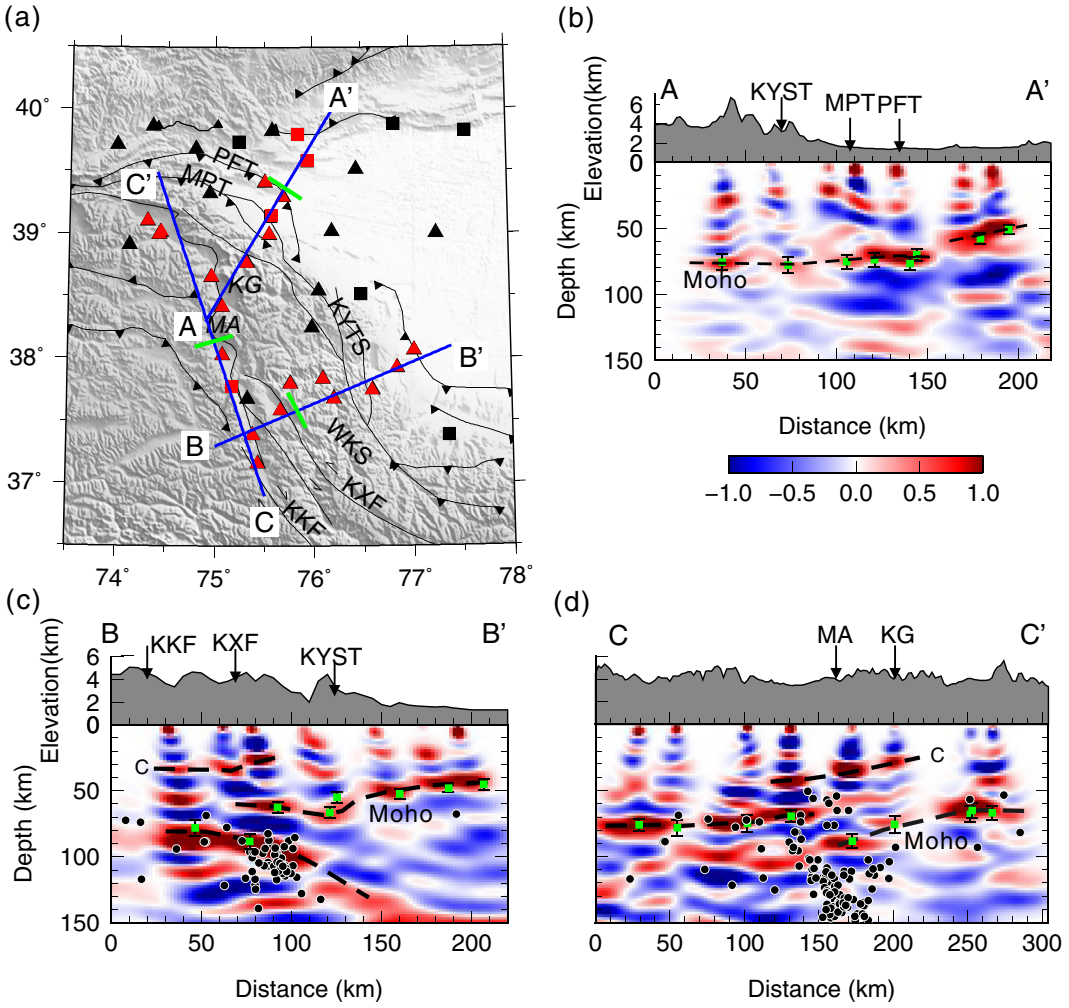

Figure 4. CCP stacking images along three cross sections, A-A′, B-B′, and C-C′. The positive (negative) amplitudes are filled in red (blue) to indicate the interfaces where the velocity increases (decreases) with depth. The resulting crustal thicknesses and errors are marked by the green squares and bars, respectively, and are superimposed on the well-resolved Moho conversions (black dashed lines). The black circles are the projected intermediate-depth earthquakes with depths greater than 50 km perpendicular to the profile within 50 km. C marks an intracrustal interface. Stations used in the three CCP cross sections are marked by red color. The green lines in Figure 4a highlight the anomalous locations of the Moho depth discussed in the text. CCP, common conversion point.

around 5–6 Ma (Thompson et al., 2015). Analogous scenarios have also been reported in the transitional regions between the South-Central Tien Shan and northern Tarim Basin (B. Zhang et al., 2020), and along the boundary between western Tibet and the southern Tarim Basin (Murodov et al., 2018). Furthermore, a similar Moho offset is absent in the North Pamir-Tien Shan collision zone, west of 75° E. The reasons for this phenomenon could be that the lithospheric strength of Tien Shan is weaker than that beneath Tarim Basin (Bagdassarov et al., 2011), and much of the shortening between North Pamir and the southern Tien Shan has migrated into the Tien Shan east of 75° E since 10 Ma (E. Sobel et al., 2006). We, therefore, propose that the manner of crustal interactions among different blocks appears to be controlled by their stiffness and density.

Previous studies have suggested the delamination of Asian lower crust beneath North and Central Pamir west of our study area (Kufner et al., 2016). Following these studies and considering the dominant E-W strike of intermediate-depth seismicity, we suggest that the Moho offset observed beneath MA represents the eastward expansion of the delaminated Asian lower crust terminating at the KYTS. The Vs model for station EP15 to the south of this Moho offset exhibits a 67 km thick crust with a lower crust of 3.8–4.1 km/s,

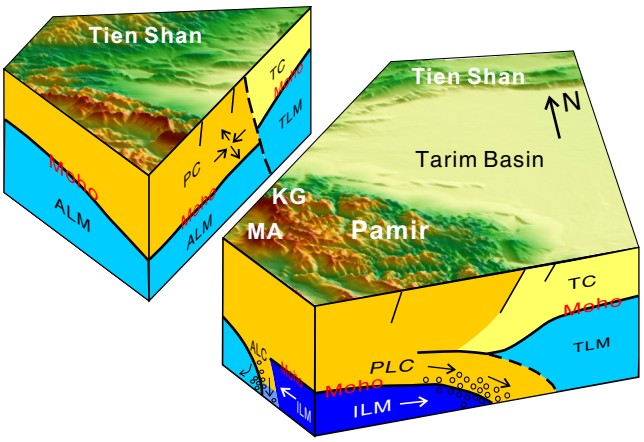

Figure 5. 3-D schematic illustration for the proposed deformation patterns beneath the east Pamir. The black circles are the symbolic intermediate-depth earthquakes. ALC, Asian lower crust; ALM, Asian lithospheric mantle; ILM, Indian lithospheric mantle; PC, Pamir crust; PLC, Pamir lower crust; TC, Tarim crust; TLM, Tarim lithospheric mantle.

whereas that for station EP14 to the north of this Moho offset shows a lower crust of 4.0 km/s reaching a depth of 88 km (Figure S4). This scenario of no overlapping Moho and sinking Asian lower crust is in more accordance with delamination than classical subduction because the downgoing Asian crust is primarily driven by the indentation of the Indian lithosphere and negative buoyancy due to the eclogitization of Asian lower crust (Kufner et al., 2016; Schneider et al., 2013).

The most intriguing structure of our observations is a double Moho in the southern portion of the east Pamir. In conjunction with the NW-SE trending intermediate-depth seismicity, we suggest that this double Moho structure provides direct evidence for eastward underthrusting of the Pamir lower crust beneath the West Kunlun Shan and Tarim Basin. The Vs model for station EP29 sampling this double Moho structure reveals a 30 km thick layer of 4.0 km/s below 70 km depth between two identified Moho interfaces (Figure S5), suggesting the presence of underthrusting mafic crustal material which can be connected to the 3.9 km lower crust of station EP30 on the southwest of this double Moho structure. Conversely, a similar structure identified below western Pamir has been interpreted to represent underthrusting of the Tajik lower crust (Schneider et al., 2019). The spatial relationship of the two Moho troughs with the intermediate-depth seismic zones implies that underthrusting involves crust. In the west Pamir, the Moho trough is located northwest of the seismic zone, suggesting a southeastward underthrusting of the Asian crust (Schneider et al., 2019). In the east Pamir, the Moho trough is to the west of the seismic zone, indicating analogically an eastward underthrusting of the Pamir crust. Our interpretation is compatible with sedimentary and magnetostratigraphic analyses along the Aertashi section, which indicate eastward-directed thrusting of the Pamir onto Tarim Basin and a rotation from approximately N-S to E-W in the maximum strain orientation at 15 Ma (Blayney et al., 2019). Crustal xenoliths from the Dunkeldik volcanic field erupted at 11 Ma in the southeastern Pamir suggest that Gondwanan Pamir crust was subducted to depths of 90–100 km beneath Eurasia (Hacker et al., 2005), which is analogous to our interpretation. A notable high-velocity anomaly imaged below 180 km depth has been interpreted as northward underthrusting Indian mantle lithosphere (Kufner et al., 2018; Liang et al., 2020), which may provide the driving force for the development of the underthrusting structure described here. Furthermore, the contrasting subduction styles in the west and east Pamir can be partly explained by the steep subduction of the Indian lithosphere under the Hindu Kush and the flat-slab underthrusting of the Indian lithospheric mantle beneath the Pamir (Kelly & Beaumont, 2021).

We also observe a positive converter at depths of 20–40 km, which is labeled by C on CCP images of profiles B-B′ and C-C′ (Figure 4). This gently dipping C corresponds to an intracrustal interface, which is also the bottom of the low velocity zone evidenced by the obtained Vs models (Figures S4 and S5). We interpret C to represent a décollement surface (Singh et al., 2010), along which the Pamir upper crust is decoupled from the underlying crust. Note that the low lateral resolution at shallow depth due to the sparse station coverage does not allow us to further discuss its implication.

Additionally, the κ values of 1.68–1.81 mainly occur at most stations of the east Pamir, station BPM in the southern Tien Shan, and station EP22 in the Tarim Basin. These low to moderate κ values suggest felsic and intermediate bulk crustal compositions probably resulted from delamination or foundering of the mafic lower crust. The high κ values of more than 1.81 in Tarim Basin are likely caused by the thick sedimentary sequences, whereas those in the east Pamir and southern Tien Shan may be the result of fractured damage zones and/or partial melt within the crust.

5. Conclusions

We obtain the crustal structure below the east Pamir and its adjacent region by applying PRF techniques to teleseismic waveforms recorded at a temporary 2-D seismic array and the permanent stations. The crustal thickness ranges from 67-88 km beneath the east Pamir and reduces to 50–60 km along the southern Tien Shan and 41–50 km in the Tarim Basin. Our depth migration images indicate the presence of a double Moho structure and two Moho offsets, which shed new light on crustal deformation patterns in the east Pamir. We suggest that pure shear shortening accounts for crustal thickening in NE Pamir, while delamination of Asian lower crust and eastward underthrusting of Pamir lower crust dominate the deformation processes in the central and southern portions of the east Pamir, respectively.

Data Availability Statement

Temporary instruments were provided by the Geophysical Instrument Pool Potsdam (GIPP). Seismic data are archived at the GEOFON data center (https://doi.org/10.14470/3U7560589977) and at the Institute of Tibetan Plateau Research, Chinese Academy of Sciences. We thank the Data Management Center of the China National Seismic Network at the Institute of Geophysics, China Earthquake Administration, for providing waveform data of permanent stations (SEISDMC, https://doi.org/10.11998/SeisDmc/SN, http://www.seisdmc.ac.cn/).

Acknowledgments
This research was funded by the Strategic Priority Research Program of Chinese Academy of Sciences (XDA20070302), the National Natural Science Foundation of China (42074113), and the CaTeNA project of the German Federal Ministry of Science and Education (support code 03G0878A). Valuable comments by Arun Singh and Lun Li helped us improve the manuscript. The temporary seismic experiment (8H) was partly supported by the expedition fund from Deutsches GeoForschungsZentrum GFZ.

References

Bagdassarov, N., Batalev, V., & Egorova, V. (2011). State of lithosphere beneath Tien Shan from petrology and electrical conductivity of xenoliths. *Journal of Geophysical Research*, *116*, B01202. https://doi.org/10.1029/2009jb007125

Blayney, T., Dupont-Nivet, G., Najman, Y., Proust, J. N., Meijer, N., Roperch, P., et al. (2019). Tectonic evolution of the Pamir recorded in the Western Tarim Basin (China): Sedimentologic and magnetostratigraphic analyses of the Aertashi section. *Tectonics*, *38*(2), 492–515. https://doi.org/10.1029/2018TC005146

Bloch, W., Schurr, B., Yuan, X., Ratschbacher, L., Reuter, S., Kufner, S. K., et al. (2021). Structure of the deep lithosphere between Pamir and Tarim. *EarthArXiv Preprints*. https://doi.org/10.31223/X5N60C

Burtman, V. S., & Molnar, P. (1993). Geological and geophysical evidence for deep subduction of continental crust beneath the Pamir. In *Geological and geophysical evidence for deep subduction of continental crust beneath the Pamir* (Vol. *281*, pp. 1–76). Geological Society of America Special Paper. https://doi.org/10.1130/spe281-p1

Hacker, B., Luffi, P., Lutkov, V., Minaev, V., Ratschbacher, L., Plank, T., et al. (2005). Near-ultrahigh pressure processing of continental crust: Miocene crustal xenoliths from the Pamir. *Journal of Petrology*, *46*(8), 1661–1687. https://doi.org/10.1093/petrology/egi030

Kelly, S., & Beaumont, C. (2021). Balanced cross-sections and numerical modeling of the lithospheric-scale evolution of the Hindu Kush and Pamir. *Journal of Geophysical Research: Solid Earth*, *126*(3), e2020JB020678. https://doi.org/10.1029/2020JB020678

Kufner, S. K., Eken, T., Tilmann, F., Schurr, B., Yuan, X., Mechie, J., et al. (2018). Seismic anisotropy beneath the Pamir and the Hindu Kush: Evidence for contributions from crust, mantle lithosphere, and asthenosphere. *Journal of Geophysical Research: Solid Earth*, *123*(12), 10727–10748. https://doi.org/10.1029/2018JB015926

Kufner, S.-K., Schurr, B., Sippl, C., Yuan, X., Ratschbacher, L., Akbar, A. s. o. M., et al. (2016). Deep India meets deep Asia: Lithospheric indentation, delamination and break-off under Pamir and Hindu Kush (Central Asia). *Earth and Planetary Science Letters*, *435*, 171–184. https://doi.org/10.1016/j.epsl.2015.11.046

Liang, Y., Li, L., Liao, J., & Gao, R. (2020). Interaction of the Indian and Asian plates under the Pamir and Hindu-Kush Regions: Insights from 3-D shear wave velocity and anisotropic structures. *Geochemistry, Geophysics, Geosystems*, *21*(8). https://doi.org/10.1029/2020GC009041

Li, Y. P., Robinson, A. C., Lapen, T. J., Righter, M., & Stevens, M. K. (2020). Muztaghata Dome Miocene Eclogite facies metamorphism: A record of lower crustal evolution of the NE Pamir. *Tectonics*, *39*, e2019TC005917. https://doi.org/10.1029/2019TC005917

Mechie, J., Schurr, B., Yuan, X., Schneider, F., Sippl, C., Minaev, V., et al. (2019). Observations of guided waves from the Pamir seismic zone provide additional evidence for the existence of subducted continental lower crust. *Tectonophysics*, *762*, 1–16. https://doi.org/10.1016/j.tecto.2019.04.007

Metzger, S., Ischuk, A., Deng, Z., Ratschbacher, L., Perry, M., Kufner, S. K., et al. (2020). Dense GNSS profiles across the Northwestern tip of the India-Asia collision zone: Triggered slip and westward flow of the Peter the First Range, Pamir, into the Tajik Depression. *Tectonics*, *39*(2), e2019TC005797. https://doi.org/10.1029/2019TC005797

Murodov, D., Zhao, J., Xu, Q., Liu, H., & Pei, S. (2018). Complex N-S variations in Moho depth and Vp/Vs ratio beneath the western Tibetan Plateau as revealed by receiver function analysis. *Geophysical Journal International*, *214*(2), 895–906. https://doi.org/10.1093/gji/ggy170

Negredo, A. M., Replumaz, A., Villaseñor, A., & Guillot, S. (2007). Modeling the evolution of continental subduction processes in the Pamir-Hindu Kush region. *Earth and Planetary Science Letters*, *259*(1–2), 212–225. https://doi.org/10.1016/j.epsl.2007.04.043

Pegler, G., & Das, S. (1998). An enhanced image of the Pamir-Hindu Kush seismic zone from relocated earthquake hypocenters. *Geophysical Journal International*, *134*(2), 573–595. https://doi.org/10.1046/j.1365-246x.1998.00582.x

Perry, M., Kakar, N., Ischuk, A., Metzger, S., Bendick, R., Molnar, P., & Mohadjer, S. (2019). Little geodetic evidence for localized Indian subduction in the Pamir-Hindu Kush of Central Asia. *Geophysical Research Letters*, *46*(1), 109–118. https://doi.org/10.1029/2018GL080065

Schmidt, J., Hacker, B. R., Ratschbacher, L., Stübner, K., Stearns, M., Kylander-Clark, A., et al. (2011). Cenozoic deep crust in the Pamir. *Earth and Planetary Science Letters*, *312*(3–4), 411–421. https://doi.org/10.1016/j.epsl.2011.10.034

Schneider, F. M., Yuan, X., Schurr, B., Mechie, J., Sippl, C., Haberland, C., et al. (2013). Seismic imaging of subducting continental lower crust beneath the Pamir. *Earth and Planetary Science Letters*, *375*, 101–112. https://doi.org/10.1016/j.epsl.2013.05.015

Schneider, F. M., Yuan, X., Schurr, B., Mechie, J., Sippl, C., Kufner, S. K., et al. (2019). The crust in the Pamir: Insights from receiver functions. *Journal of Geophysical Research: Solid Earth*, *124*(8), 9313–9331. https://doi.org/10.1029/2019JB017765

Schurr, B., Ratschbacher, L., Sippl, C., Gloaguen, R., Yuan, X., & Mechie, J. (2014). Seismotectonics of the Pamir. *Tectonics*, *33*(8), 1501–1518. https://doi.org/10.1002/2014TC003576

Schwab, M., Ratschbacher, L., Siebel, W., McWilliams, M., Minaev, V., Lutkov, V., et al. (2004). Assembly of the Pamirs: Age and origin of magmatic belts from the southern Tien Shan to the southern Pamirs and their relation to Tibet. *Tectonics*, *23*(4). https://doi.org/10.1029/2003TC001583

Singh, A., Kumar, M. R., & Raju, P. S. (2010). Seismic structure of the underthrusting Indian crust in Sikkim Himalaya. *Tectonics*, *29*. https://doi.org/10.1029/2010tc002722

Sippl, C., Schurr, B., Tympel, J., Angiboust, S., Mechie, J., Yuan, X., et al. (2013). Deep burial of Asian continental crust beneath the Pamir imaged with local earthquake tomography. *Earth and Planetary Science Letters*, *384*, 165–177. https://doi.org/10.1016/j.epsl.2013.10.013

Sippl, C., Schurr, B., Yuan, X., Mechie, J., Schneider, F. M., Gadoev, M., et al. (2013). Geometry of the Pamir-Hindu Kush intermediate-depth earthquake zone from local seismic data. *Journal of Geophysical Research: Solid Earth*, *118*(4), 1438–1457. https://doi.org/10.1002/jgrb.50128

Sobel, E., Chen, J., & Heermance, R. (2006). Late Oligocene-Early Miocene initiation of shortening in the Southwestern Chinese Tian Shan: Implications for Neogene shortening rate variations. *Earth and Planetary Science Letters*, *247*(1–2), 70–81. https://doi.org/10.1016/j.epsl.2006.03.048

Sobel, E. R., Chen, J., Schoenbohm, L. M., Thiede, R., Stockli, D. F., Sudo, M., & Strecker, M. R. (2013). Oceanic-style subduction controls late Cenozoic deformation of the Northern Pamir orogen. *Earth and Planetary Science Letters*, *363*, 204–218. https://doi.org/10.1016/j.epsl.2012.12.009

Thompson, J. A., Burbank, D. W., Li, T., Chen, J., & Bookhagen, B. (2015). Late Miocene northward propagation of the northeast Pamir thrust system, northwest China. *Tectonics*, *34*(3), 510–534. https://doi.org/10.1002/2014TC003690

Xu, Q., Zhao, J., Yuan, X., Liu, H., & Pei, S. (2017). Detailed configuration of the underthrusting Indian lithosphere beneath Western Tibet revealed by receiver function images. *Journal of Geophysical Research: Solid Earth*, *122*(10), 8257–8269. https://doi.org/10.1002/2017JB014490

Yuan, X., Ni, J., Kind, R., Mechie, J., & Sandvol, E. (1997). Lithospheric and upper mantle structure of southern Tibet from a seismological passive source experiment. *Journal of Geophysical Research*, *102*(B12), 27491–27500. https://doi.org/10.1029/97jb02379

Yuan, X., Schurr, B., Bloch, W., Xu, Q., & Zhao, J. (2018). *The 8H East Pamir seismic network*. GFZ Data Services. https://doi.org/10.14470/3U7560589977

Yuan, X., Sobolev, S. V., Kind, R., Oncken, O., Bock, G., Asch, G., et al. (2000). Subduction and collision processes in the Central Andes constrained by converted seismic phases. *Nature*, *408*(6815), 958–961. https://doi.org/10.1038/35050073

Zhang, B., Bao, X., & Xu, Y. (2020). Distinct orogenic processes in the South- and North-Central Tien Shan from receiver functions. *Geophysical Research Letters*, *47*(6), e2019GL086941. https://doi.org/10.1029/2019GL086941

Zhang, X. K., Zhao, J. R., Zhang, C. K., Ren, Q. F., Nie, W. Y., & Cheng, S. X. (2002). Crustal structure at the northeast side of the Pamirs. *Chinese Journal of Geophysics-Chinese Edition*, *45*(5), 665–671. https://doi.org/10.1002/cjg2.283

Zheng, X.-F., Yao, Z.-X., Liang, J.-H., & Zheng, J. (2010). The role played and opportunities provided by IGP DMC of China National Seismic Network in Wenchuan earthquake disaster relief and researches. *Bulletin of the Seismological Society of America*, *100*(5B), 2866–2872. https://doi.org/10.1785/0120090257

Zhu, L., & Kanamori, H. (2000). Moho depth variation in southern California from teleseismic receiver functions. *Journal of Geophysical Research*, *105*(B2), 2969–2980. https://doi.org/10.1029/1999JB900322